Journal of Power Sources 196 (2011) 3470–3478

Contents lists available at ScienceDirect

Journal of Power Sources

journal homepage: www.elsevier.com/locate/jpowsour

# Tuning transport properties by manipulating the phase segregation of tetramethyldisiloxane segments in modified polyimide electrolytes

Chi-Yung Tseng[a], Yun-Sheng Ye[a], Jorphin Joseph[a], Kuei-Yu Kao[a], John Rick[a], Shou-Ling Huang[b], Bing-Joe Hwang[a,c,*]

[a] Nanoelectrochemistry Laboratory, Department of Chemical Engineering, National Taiwan University of Science and Technology, Taipei 106, Taiwan, ROC
[b] Department of Chemistry, National Taiwan University, Taipei 106, Taiwan, ROC
[c] National Synchrotron Radiation Research Center, Hsinchu 300, Taiwan, ROC

ARTICLE INFO

*Article history:*
Received 24 October 2010
Received in revised form 1 December 2010
Accepted 6 December 2010
Available online 14 December 2010

*Keywords:*
Proton conductor
Sulfonated polyimide
Composite membrane
Fuel cells
Phase separation

ABSTRACT

A series of copolymer electrolytes containing 4,4′-oxydianiline (ODA)-based sulfonated polyimide and siloxane segments, in various ratios, are prepared and characterized for direct methanol fuel cell applications. The chemical Structure of the sulfonated copolymers is confirmed by FT-IR and NMR. The prepared composite membranes are found to be flexible and show good thermal stability as well as good proton conductivity. A maximum proton conductivity of $5.78 \times 10^{-2}$ S cm$^{-1}$ (cf. Nafion117 = $8.31 \times 10^{-2}$ S cm$^{-1}$) is obtained for the sulfonated polyimide blended with sulfonated polyimide with a grafted tetramethyldisiloxane segment (cf. SPI_DSX75 membrane) at 90 °C. The membranes showed low methanol crossover below $10^{-7}$ cm$^2$ s$^{-1}$ (cf. Nafion117 = $10^{-6}$ cm$^2$ s$^{-1}$). The transport properties of the membranes are found to be strongly influenced by water uptake and by the number and nature of the ionic clusters in the hydrophilic domains. When the number of siloxane segments is increased, the relationship between the methanol self-diffusion coefficient ($D_M$) and water molecules per sulfonic acid group ($\lambda$) indicate that the water molecules are interacting with channels inside the membrane. In addition, the segregated nanophase also affects the ion transport and sometimes enhances the corresponding ionic conductivity. TEM and SAXS analyses shows evidence for phase segregation in the membranes and reveal the influence of flexible siloxane segments in ionic clustering.



## 1. Introduction

Functionalized polymers are gaining importance in advanced technologies, such as proton exchange membrane fuel cells (PEMFCs). Until now, perfluorosulfonated polymers, such as DuPont's Nafion membrane, remain the benchmark polymers for PEMFCs. Besides their excellent thermal and mechanical properties, these materials show reasonably good proton conductivity in humidified conditions at intermediate temperatures. But these materials have some drawbacks such as: high methanol crossover, and loss of conductivity at temperatures above 100 °C [1,2]. Currently, much research is directed towards obtaining membranes that overcome these problems.

Various sulfonated aromatic polymers, such as: poly(aryl ether sulfone) [3–6], poly(ether ketone) [7,8], polyimide (PI) [9–18], Polybenzimidazole (PBI) [19–23], etc. have been proposed as alternative membrane materials. However, most of the sulfonated aromatic polymers and acid-doped polymers have lower proton conductivities in comparison to Nafion, although few of them exhibit enhanced mechanical properties or lower methanol permeability. The proton conductivity of polymer membranes depends on the: chemical structure of the polymer, its ion exchange capacity (IEC), and its water uptake and hydrated morphology. The study of phase separation in polymer electrolyte membranes has emphasized the significance of the formation of ionic channels to improve proton conductivity. Nafion is usually made with a polytetrafluoroethylene backbone and perfluorinated vinyl ether pendant side chains terminated by a sulfonate ionic group [24]. Upon hydration, phase separation occurs between the hydrophobic region and the hydrophilic ionic domains in Nafion [25]. In general, sulfonated aromatic polymers have a lower hydrophilic/hydrophobic difference and a more rigid polymer backbone, both of which lead to the formation of narrower hydrophilic channels with more dead-end pockets as compared to Nafion. Considerable advances have been made in the design of polymer electrolytes by manipulating the ordering and distribution of ionic clusters to achieve phase segregation and connectivity. Silica-based organic-inorganic hybrids with covalent bonds, or weak physical bonds, between the inorganic

* Corresponding author at: Nanoelectrochemistry Laboratory, Department of Chemical Engineering, National Taiwan University of Science and Technology, Taipei 106, Taiwan, ROC. Tel.: +886 2 27376624; fax: +886 2 27376644.
*E-mail address:* bjh@mail.ntust.edu.tw (B.-J. Hwang).

0378-7753/$ – see front matter © 2010 Elsevier B.V. All rights reserved.
doi:10.1016/j.jpowsour.2010.12.006

**Table 1**
Characterization of IEC, water uptake, composition of state of water and activation energy ($E_a$) of composite membranes and Nafion117.

| Polymer code | Composition (wt%) | | | IEC (mequiv $g^{-1}$) | λ ($nH_2O$/$SO_3H$) | Water uptake (%) | Free water ratio (%) [free/total][a] | Bound water ratio (%) [bound/total][a] | $E_a$ (kJ $mol^{-1}$)[b] |
|---|---|---|---|---|---|---|---|---|---|
| | SPI | SPI_DSX | PI_ DSX | | | | | | |
| SPI | 100 | 0 | 0 | 1.73 | 12.42 | 38.85 | 6.04 | 93.96 | 33.91 |
| SPI_DSX10 | 90 | 10 | 0 | 1.71 | 13.08 | 40.33 | 7.31 | 92.69 | 26.89 |
| SPI_DSX20 | 80 | 20 | 0 | 1.66 | 14.27 | 42.88 | 8.75 | 91.25 | 25.93 |
| SPI_DSX30 | 70 | 30 | 0 | 1.61 | 16.81 | 48.87 | 9.18 | 90.82 | 25.59 |
| SPI_DSX40 | 60 | 40 | 0 | 1.56 | 19.10 | 53.81 | 11.33 | 88.67 | 28.18 |
| SPI_DSX50 | 50 | 50 | 0 | 1.55 | 21.30 | 59.43 | 13.69 | 86.31 | 27.38 |
| SPI_DSX75 | 25 | 75 | 0 | 1.51 | 34.36 | 93.71 | 32.89 | 67.11 | 35.91 |
| SPI_DSX100 | 0 | 100 | 0 | 1.53 | -[c] | -[c] | -[c] | -[c] | -[c] |
| PI_DSX50 | 50 | 0 | 50 | 0.83 | 11.74 | 17.67 | 11.26 | 88.74 | 8.99 |
| Nafion117 | – | – | – | 0.91 | 21.97 | 36 | NM | NM | 18.31 |

"NM" not measured.
[a] Obtained using DSC.
[b] The activation energy derived from the proton conductivity measurement in the temperature range of 30–90 °C in water.
[c] Mechanically unstable.

(siloxane) and organic phases have been extensively studied in this regard [26–28]. The properties of such polymer blends strongly depend on the interactions between the inorganic and organic phases.

This study focuses on the transport properties of copolymers. Polymer electrolyte membranes were prepared by blending 4,4′-oxydianiline (ODA)-based sulfonated polyimide (SPI) with a diamine bearing a 1,3-bis (3-aminopropyl) tetramethyldisiloxane, together with a sulfonated form of the same diamine. 1,4,5,8-Naphthalenetetracarboxylic dianhydride (NTDA) was chosen as the dianhydride monomer because its naphthalimide rings exhibit an improved hydrolytic stability in comparison to phthalimide rings [29]. Commercially available 2,2-Benzidinedisulfonic acid (BDSA) was used for the introduction of the sulfonic acid groups. The flexibility of the siloxane segments was expected to inhibit the formation of a dense, well packed polyimide structure. Sulfonated polyimides without siloxane segments were also prepared using ODA for comparison: such ODA based polyimides are reported to have good film-forming ability [11,14–17].

## 2. Experimental

### 2.1. Materials

1,4,5,8-Naphthalenetetracarboxylic dianhydride (NTDA) and 4,4′-oxydianiline (ODA) were purchased from Aldrich and purified by vacuum sublimation before use. Triethylamine (TEA) was dried using molecular sieves of 4 Å. 1,3-bis (3-aminopropyl) tetramethyldisiloxane (DSX) was purchased from Alfa Aesar. 2,2-Benzidinedisulfonic acid (BDSA; 70%, TCI) was dispersed in ethanol and was neutralized by adding triethylamine at 60 °C until it dissolved completely. BDSA_$Et_3$HN was purified by recrystallization from ethanol solution and was dried under vacuum for 48 h. Benzoic acid and m-cresol were purchased from Acros and used as received.

### 2.2. Synthesis

ODA-based sulfonated polyimide (SPI) was synthesized as described elsewhere [11,14–16]. In a typical experiment, BDSA-$Et_3$HN (8 mmol), ODA (8 mmol) and m-cresol (50 ml) were add to a three-neck flask with stirring under nitrogen flow. After complete dissolution, NTDA (16 mmol) and Benzoic acid (22.4 mmol) were added to the flask. The mixture was stirred at room temperature for 30 min, heated at 90 °C for 3 h, and then heated at 180 °C for 20 h. After cooling to room temperature, an additional 20 ml of m-cresol was added to dilute the highly viscous solution. Then the reaction mixture was poured into acetone, and the resulting fiber-like precipitate was collected by filtration and dried in vacuum at 80 °C for 20 h. Elemental analysis results: calculated for SPI in TEA form ($C_{64}H_{54}N_6O_{15}S_2$): C: 63.41%, H: 4.45%, N: 6.93%, and S: 5.28%. Found: C: 62.88%, H: 4.62%, N: 6.86%, and S: 5.22%.

The DSX-based sulfonated polyimide with grafted tetramethyldisiloxane (SPI_DSX) was also prepared using a similar procedure to that above. Elemental analysis results: calculated for SPI_DSX in TEA form ($C_{62}H_{70}N_6O_{15}S_2Si_2$): C: 59.09%, H: 5.56%, N: 6.67%, and S: 5.08%. Found: C: 60.14%, H: 5.71%, N: 6.77%, and S: 5.11%.

DSX-polyimide (PI_DSX), with a composition of NTDA (50 mol%)/DSX (50 mol%), was prepared in a similar way to the ODA-based sulfonated polyimide. Elemental analysis results: Calculated for PI_DSX ($C_{24}H_{30}N_2O_5Si_2$): C: 59.75%, H: 6.22%, and N: 5.81%. Found: C: 59.74%, H: 6.28%, and N: 5.83%.

### 2.3. Preparation of composite membranes

The composite membranes were prepared by a solvent-casting method. Calculated amounts of SPI and SPI_DSX (or PI_DSX) were mixed with the required amounts of m-cresol to form 5% solutions under nitrogen purging [a notation SPI_DSX50 in the manuscript implies a blend sample containing 50 wt% SPI_DSX (or PI_DSX) derivatives (Table 1)]. The solution was poured onto a glass plate to form membranes, which were heated slowly at 80 °C for 1 h, 100 °C for 3 h, and finally 120 °C for 10 h, to remove most of the solvent. The dried films were soaked in methanol at room temperature for 24 h to remove the residual solvent and then the proton exchange membrane treatment was performed by immersing the membranes in 1 M $H_2SO_4$ at room temperature for 24 h. The proton exchange membranes were thoroughly washed with deionized water until a neutral pH was reached. The thickness of the prepared membranes was in the range 20–40 μm.

### 2.4. Measurements

Fourier transform infrared (FTIR) spectra were determined with a Bio-Rad FTS-3500 spectrometer from 4000 to 400 $cm^{-1}$. $^1$H NMR spectra were recorded on a Bruker Advance-500 MHz FT-NMR spectrometer using deuterated dimethyl sulfoxide (DMSO-$d_6$) as a solvent and tetramethylsilane (TMS) as an internal standard. Thermogravimetric analyses (TGA) were run on a Perkin Elmer pyres 1 instrument under a continuous nitrogen flow. The acid form sam-

ples were preheated (100 °C for 30 min) to remove the moisture. TGA curves were recorded in the range 100–900 °C, at a heating rate of 10 °C min$^{-1}$. Differential scanning calorimetry (DSC) measurements were carried out using a DSC Q100 instrument (TA Instruments) calibrated against indium. Fully hydrated membrane samples (about 8–10 mg total mass per sample) were wiped gently with paper to remove superficial water and then immediately placed into an aluminum pan and sealed. The samples were held at −100 °C for 1 min and then heated to 100 °C, at a heating rate of 5 °C min$^{-1}$ using nitrogen as the carrier gas (flow rate 50 ml min$^{-1}$).

### 2.5. Ion exchange capacity

The ion exchange capacity (IEC) of the SPI composite membranes was measured by titration. A piece of a SPI composite membrane was equilibrated in 1 M NaCl aqueous solution for 48 h to release $H^+$ ions ($H^+$ ions in the membrane were replaced by $Na^+$ ions) into solution, where they were titrated with a standard 0.01 M NaOH aqueous solution, using phenolphthalein indicator.

### 2.6. Proton conductivity

Proton conductivity in the plane direction of membrane was determined using an electrochemical impedance spectroscopy technique over the frequency range 1 kHz–1 MHz, using a Parstat 2263 potentiostat (Advanced Electrochemical System Instruments). Each sample was cut into strips that were approximately 2 cm wide and 2 cm long, prior to being mounted on the cell. The resistance of each SPI composite membrane was measured, at a temperature in the range (30–90 °C), and the value of the proton conductivity ($\sigma$) determined from formula:

$$\sigma = \frac{d}{SR}$$

Where $d$ is the thickness of the membrane, $S$ is the area of the interface between the membrane and the electrode, and $R$ is the measured resistance of the membrane.

### 2.7. Water uptake – methanol uptake – dimensional change and λ

The membrane was vacuum dried at 100 °C for 24 h and weighed, prior to immersion in water, or methanol, at room temperature. The wet membrane was quickly wiped to remove surface water (or methanol) and weighed again. The water uptake of the membrane was calculated using Eq. (1):

$$\text{Water uptake} = (\%) = \frac{W_w - W_d}{W_d} \times 100\% \quad (1)$$

where $W_w$ and $W_d$ are the weights of the corresponding water, wet and dry, membranes, respectively.

The methanol volume fraction ($\phi_M$) was calculated using Eq. (2):

$$\phi_M = \frac{W_w^M - W_d^M}{V_w^M \cdot \rho_M} \quad (2)$$

where $W_w^M$ and $W_d^M$ are the weights of the corresponding methanol, wet and dry, membranes respectively. $V_w^M$ and $\rho_M$ are respectively the volume of the membrane soaked in methanol and the density of methanol.

The number of water molecules per ionic group ($\lambda$) can be determined from the water uptake and the IEC of the membrane using Eq. (3):

$$\lambda = \frac{n(H_2O)}{n(SO_3^-)} = \frac{\text{Water Uptake}}{M_{WH_2O} \cdot \text{IEC}} \times 1000 \quad (3)$$

where $n(H_2O)$ is the $H_2O$ mole number, $n(SO_3^-)$ is the $SO_3^-$ group mole number, and $M_{WH_2O}$ is the molecular weight of water.

### 2.8. Methanol permeability

A glass diffusion cell was used to determine the methanol permeability of the composite membranes. This cell consisted of two reservoirs, each with a capacity of approximately 50 ml, separated by a vertical membrane. One side ($V_A$) of the cell was filled with 10 wt% methanol; the other contained deionized water ($V_B$): during measurement the reservoir's contents were subject to magnetic stirring. As methanol permeation proceeded, the concentration of methanol in the water reservoir increased: this was detected using gas chromatography with a thermal conductivity detector (FID, 8700F). The permeability of methanol was calculated by analyzing the methanol flux, with respect to time, and applying the formula (4):

$$C_B(t) = \frac{A}{V_B} \times \frac{DK}{L} \times C_A \times (t - t_0) \quad (4)$$

where $C_A$ and $C_B$ respectively represent the methanol concentrations in the methanol reservoir and in the water reservoir; $DK$ is the methanol diffusion coefficient (cm$^2$ s$^{-1}$); $V_B$, $A$ (cm$^2$) and $L$ (cm) are the volume of the permeated reservoir, the effective area, and the thickness of membrane respectively.

The investigation assumes that $D$ in the membrane is constant and that $K$ is independent of concentration. The product $DK$ is the membrane permeability [$P$ (cm$^2$ s$^{-1}$)]. P was obtained from the following Eq. (5):

$$P = \frac{1}{A} \times \frac{C_B(t)}{C_A(t - t_0)} \times V_B L \quad (5)$$

$C_B$ was measured several times during the permeation experiment to enable the methanol permeability to be obtained from the slope of the straight line.

Methanol self-diffusion coefficients ($D_M$) is calculated by Eq. (6) [30]:

$$D_M = \frac{P}{\phi_M} \quad (6)$$

where $P$ is the methanol permeability, $\phi_M$ is the methanol volume fraction.

### 2.9. TEM characterizations

The protonated form of the composite membrane was converted into the -$SO_3Ag$ form by immersing it in 0.5 M $AgNO_3$ solution for 12 h, it was then thoroughly washed with deionized water and dried at room temperature for 24 h. The dried samples were encapsulated in epoxy resin and cross-sectioned in a microtome to yield 80 nm thick sections. The samples were imaged in a Philips Technai G2 TEM at two different magnifications. Darker areas in the micrographs are associated with Ag containing, hydrophilic domains.

### 2.10. Small angle X-ray scattering (SAXS) measurements

SAXS experiments were performed using the BL23A SWAXS instrument at the National Synchrotron Radiation Research Center (NSRRC), Taiwan, using a 10 keV (wavelength λ = 1.24 Å) beam with a 0.5 nm diameter. The scattering wave vector transfer function $q = 4\pi\lambda^{-1} \sin\Theta$, is defined by λ and the X-ray's scattering angle $2\Theta$. Samples for SAXS (thickness = 150–200 μm) were sealed between two thin Kapton windows (80 μm thickness each), and measured at ambient temperature (~26 °C).

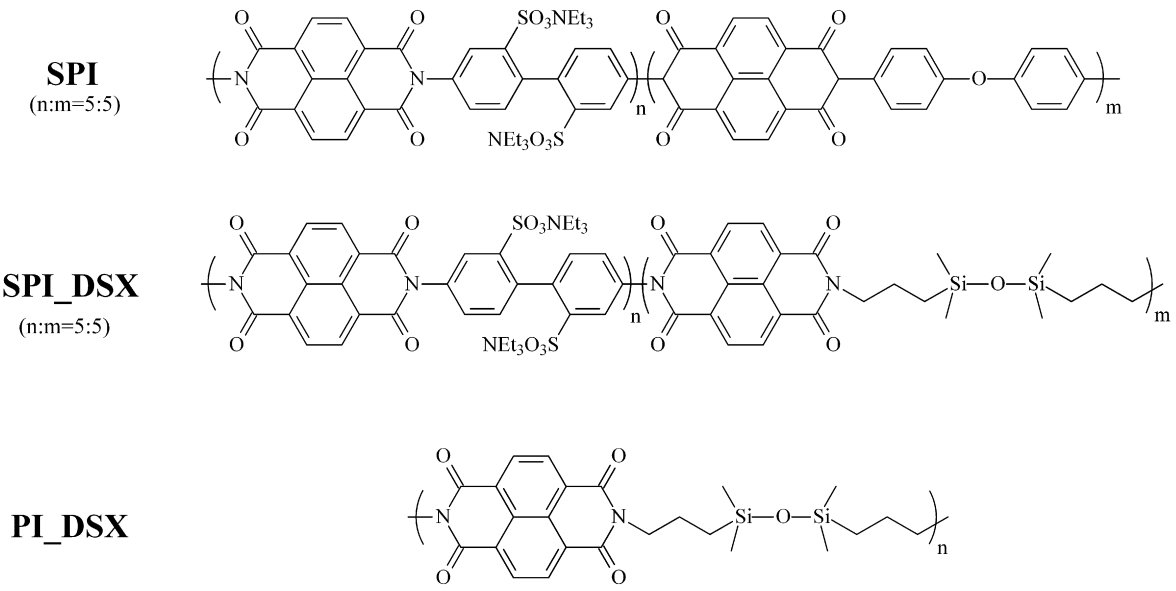


**Scheme 1.** Structures of SPI, SPI_DSX, and PI_DSX.

## 3. Result and discussion

### 3.1. Characterization of composite membrane

The chemical structure (Scheme 1) was confirmed by $^1$H NMR and FT-IR spectroscopy. Fig. 1 shows the $^1$H NMR spectrum of SPI_DSX. The peaks appearing at $\delta$ 8.75–8.89 ppm are assigned to the hydrogen atoms ($H_1$ and $H_1'$) of NTDA, while the $\delta$ 0.02 and $\delta$ 0.09 ppm resonances are from the $H_5$ and $H_5'$ hydrogen atoms of DSX. The signals due to the three methylene groups ($H_6$, $H_7$ and $H_8$) of the amino propyl moiety, on the siloxane segment, are located at $\delta$ 4.05, $\delta$ 1.71 and $\delta$ 0.59 ppm respectively. The FT-IR spectra of the SPI, SPI_DSX and PI_DSX are depicted in Fig. 2. The peaks around 1713 cm$^{-1}$ ($\nu_{sym}$ C=O), 1671 cm$^{-1}$ ($\nu_{asym}$ C=O) and 1345 cm$^{-1}$ ($\nu_{C-N-C}$ imide) are attributed to naphthalenic imide rings. The peaks at 1201, 1098, and 1032 cm$^{-1}$, correspond to the stretching vibrations of the O=S=O bond of the sulfonic acid group ($Et_3HN$ form). The $\nu$Si–O–Si stretching around 1087 cm$^{-1}$ is masked by the overlapping peaks of sulfonic acid groups appearing in the same region [31,32]. The Bands at 2096, 1377, and 785 cm$^{-1}$, originating from the DSX of the siloxane segment are $\nu CH_2$ or $\nu CH_3$, $\delta CH_3$ and $\nu$Si–$CH_3$ respectively.

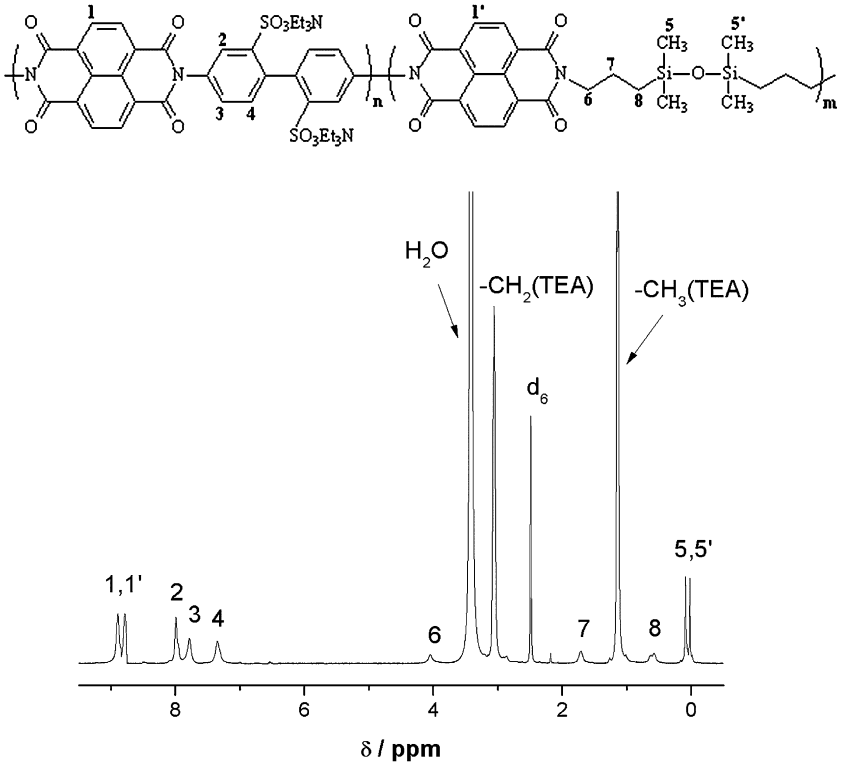


**Fig. 1.** The $^1$H-NMR spectrum of SPI_DSX.

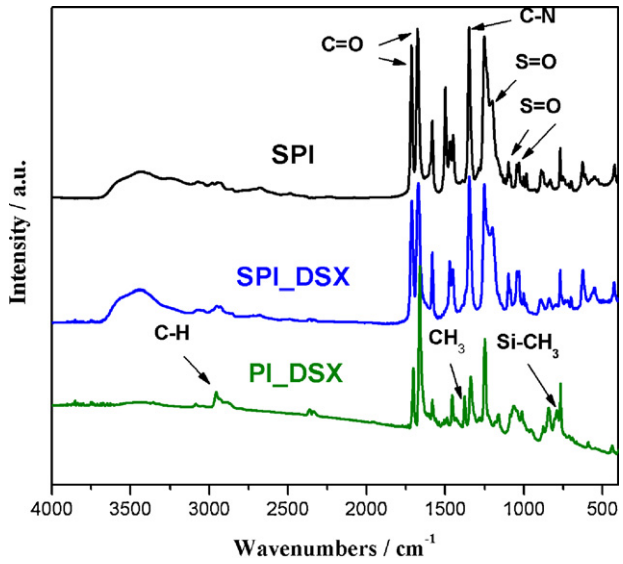


**Fig. 2.** The FTIR spectrum of SPI, SPI_DSX, and PI_DSX.

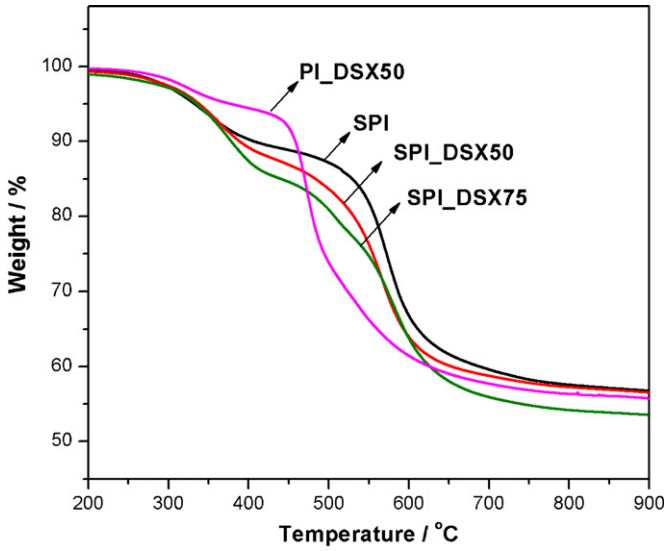


**Fig. 3.** TGA thermodiagram, temperature held under 100 °C for 30 min and then raised to 900 °C.

### 3.2. Thermal properties of the membranes

The thermal stability of the composite membranes was examined by thermo gravimetric analysis (TGA). Fig. 3 shows TGA results of the composite membranes after heating at 100 °C for 30 min to remove the moisture. The initial weight loss observed from 220 °C to 450 °C can be attributed to loss of sulfonic acid groups and siloxane segments. The introduction of siloxane segments into the rigid polyimide structure decreased the thermal stability. Thus, the SPI without siloxane segments exhibits the highest stability. Higher concentrations of siloxane segments, decrease thermal stability gradually as was observed in some previous reports [32,33]. The final weight loss with the onset temperature at about 500 °C, corresponds to the degradation of the main backbone.

### 3.3. Morphology analysis

Nanoscopic phase segregation occurs in fuel cell membrane systems because of the coexistence of hydrophobic and hydrophilic segments, which can influence such properties as proton conductivity and water uptake. The results of our morphological investigation indicate that phase segregation affects the density and size of ionic clusters. Fig. 4-1 shows TEM micrographs of: (a) SPI, (b) SPI_DSX10, (c) SPI_DSX30, (d) SPI_DSX50 (e) SPI_DSX75, (f) SPI_DSX100 and (g) PI_DSX50 membranes, where the darker regions represent localized hydrophilic ionic clusters containing protons exchanged with silver ions, while the lighter parts represent hydrophobic regions. Fig. 4-1(a) exhibits ionic clusters with a relatively uniform size (~5 nm). The size of hydrophilic ionic clusters is seen to increase, from 5 to 15 nm, with an increase in the SPI_DSX content [Fig. 4-1(b)–(e)]. In Fig. 4-1(f), i.e. SPI_DSX100 a large number of smaller ionic clusters (~5 nm) and some bigger clusters (~60 nm) are present, together with the medium sized clusters. The added SPI_DSX causes slight aggregation of the hydrophilic domains as observed by the larger black dots in the micrographs. The more flexible siloxane segments increase the mobility of ionic groups and favor rearrangements that give rise to larger clusters and pronounced segregation between hydrophobic and hydrophilic phases (as illustrated in Scheme 2). Such phase separation is also confirmed by the film transparency. The $Et_3N$-form of SPI_DSX75 was found to be transparent while the H-form of the membrane was opaque due to the evident phase separation as hydrophilic and hydrophobic domain. However, the PI_DSX50 [Fig. 4-1(g)] contains mostly larger clusters between 100 and 200 nm. The added PI_DSX without hydrophilic sulfonic acid units causes aggregation into larger ionic clusters that form isolated domains with little connectivity.

EDX results confirm the morphological features mentioned above (Fig. 4-2), by differentiating the particle components in PI_DSX50 and elucidating the component interactions for the composite membranes. Position 1 corresponds to the hydrophilic domains due to the contribution from SPI. Position 2 shows that the composite membranes have a silica content dispersed within the polymer. These changes in the morphology can affect the ionic and molecular transport through the membranes. However, the composite membranes formed with both SPI and SPI_DSX, showed a homogeneous morphology. In addition, the membrane formed with SPI and PI_DSX showed significant aggregation, possibly due to the higher hydrophobic nature of flexible siloxane moiety.

### 3.4. Ionic exchange capacity (IEC), λ, water content

Many important properties of the polymer electrolyte membranes such as the proton conductivity and water uptake depend on the IEC of the membranes, which is an indication of the amount of ion exchange sites available for carrying protons. In this study, the IEC values of the composite membranes decreased with the increase in the SPI_DSX content (Table 1), because the SPI_DSX fraction contains less sulfonic acid groups. The water uptake/IEC data were converted to the number of absorbed water molecules per sulfonic acid group (λ). Higher λ values imply higher water affinity. The λ values for composite membranes with IEC of 1.71–1.51 mequiv $g^{-1}$ is in the range of 12–34. Generally, water uptake increases as IEC increases. Interestingly, in our case, we observed the reverse tendency. Fig. 5 shows the effect of the SPI_DSX content on the water uptake and IEC. In all cases, the water uptake increases (WU of 38.85–93.71% for IEC: 1.71–1.5 mequiv $g^{-1}$) with an increase in the amount of SPI_DSX, even if the IEC decreased; which thought to result from siloxane segments in this structure reducing 'crowding' in the polymer, thus hindering molecular packing. Consequently, the amount of water molecules absorbed inside the composite membranes increased as SPI_DSX content increased. It was also noted that the ***d***-spacing increased, implying that the average distance between polymer chains might be broadened allowing vacant spaces to accommodate

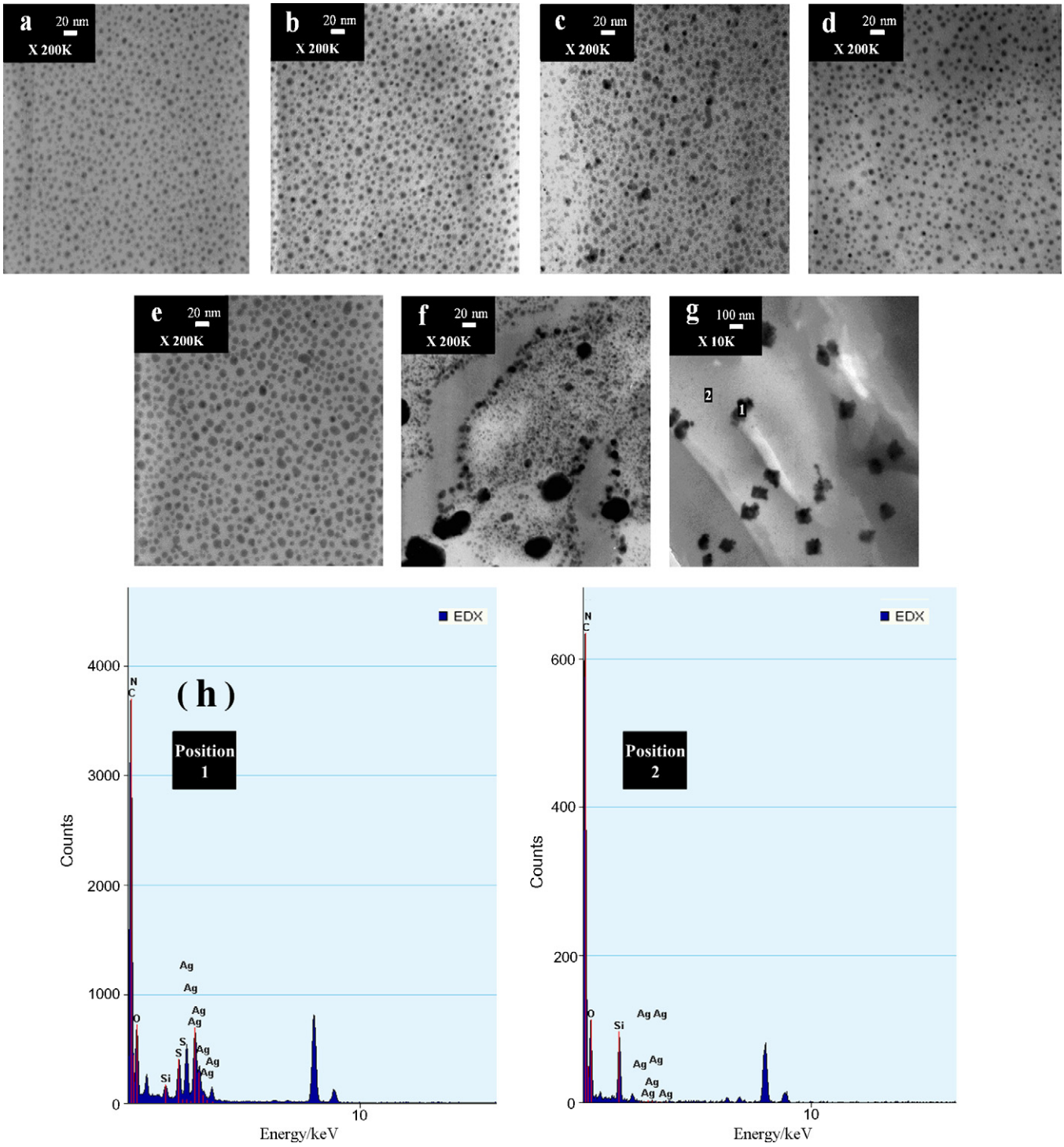


**Fig. 4.** (1) TEM micrographs of composite membrane: (a) SPI, (b) SPI_DSX10, (c) SPI_DSX30, (d) SPI_DSX50, (e) SPI_DSX75, (f) SPI_DSX100, (g) PI_DSX50. (2) EDX analysis for the image [1(g)] at (a) position 1 and (b) position 2.

more water molecules. This trend was closely related to the change of the ***d***-spacing value obtained from SAXS measurement (Table 2). However, the PI_DSX50 does not exhibit correlation ***d***-spacing, as a consequence of not having sufficient ionic clusters homogeneously dispersed to generate an observable defined ionomer peak [34]. Thus, the capacity of the membrane to contain water molecules within the polymeric structure needs to be considered when designing the polymer.

Low temperature DSC measurements are used to characterize the water associated with hydrophilic polymers. This method of analysis classifies water into either free or bound water. Free water, which is defined as the water weakly bound to the polymer, exhibits similar thermal transitions to those of bulk water. Bound water is defined as water which is strongly bound to either the polymer chain or the ionic groups that are associated with the polymer [35,36]. The water state (i.e. the free and bound water ratios of the total water content) of fully hydrated membranes is summarized in Table 1. For composite membranes, the free water ratio increases with the SPI_DSX content. This is clearly due to the presence of more vacant spaces accommodating water molecules resulting in

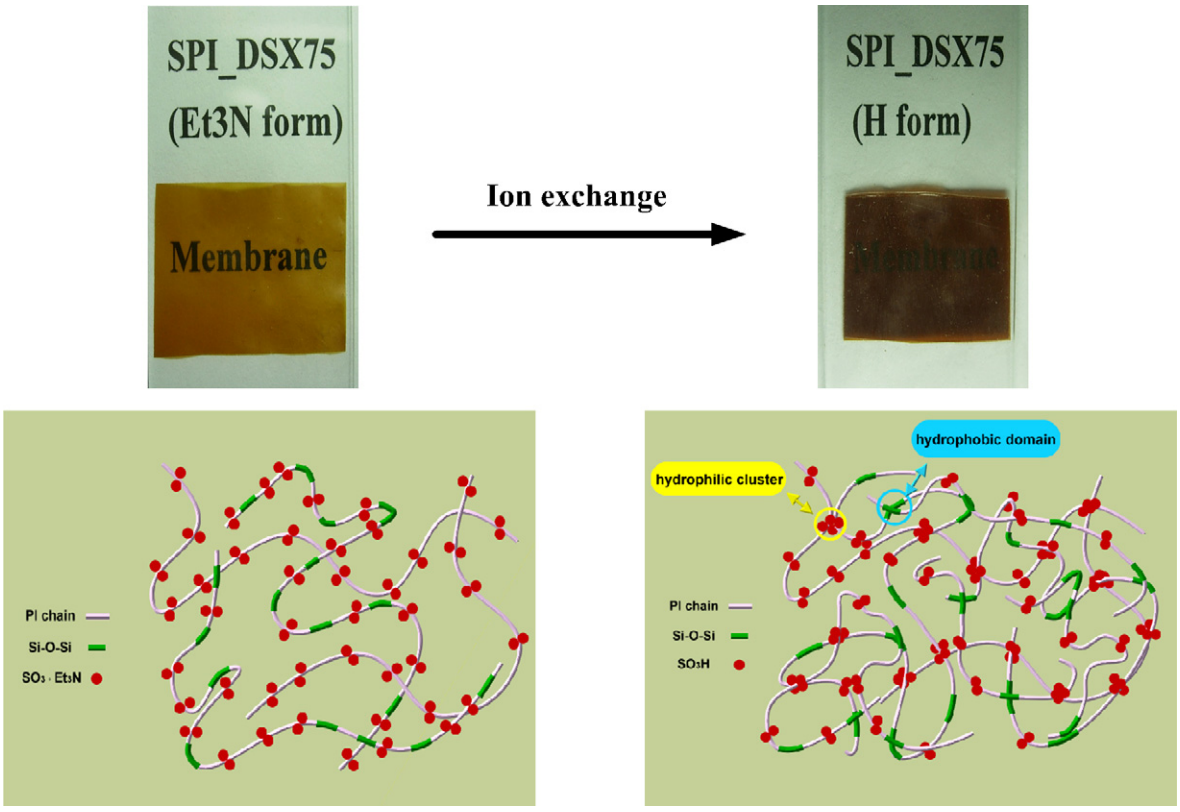


**Scheme 2.** Scheme showing the segregation of hydrophilic/hydrophobic domains in the prepared membrane.

a relatively weak water-polymer interaction around the sulfonic group. This feature may accelerate the proton transport by favoring the vehicle mechanism. However, the influence of water uptake values with the introduction of sulfonic acid groups and IEC in proton exchange membranes is not a single and primary factor that by itself increases proton conductivity.

### 3.5. Proton conductivity

The proton conductivity of the composite membranes was determined as a function of temperature (30–90 °C) at 100% relative humidity. Fig. 6 shows temperature vs. conductivity plots for the prepared composite membranes. The proton conductivity of the composite membranes and Nafion117 increased with an increase in temperature. An increase in temperature favors the dynamics involved in proton transfer and the structural reorganization that are required for fast proton conductivity. Increased temperatures favor both the structural and vehicular diffusion of protons resulting in increased proton conductivity [15]. Proton transport in membranes requires well connected channels formed by ionic clusters of hydrophilic sulfonic acid groups. The size and distribution of ionic clusters has a significant effect on the selective transport of protons through the membranes. The SPI_DSX series of membranes showed higher proton conductivity than the SPI membranes throughout the whole temperature range, signifying that larger ionic clusters can facilitate faster proton diffusion. The increasing contents of siloxane segments from SPI_DSX allowed ionic groups (sulfonic acids) to move together to form large ionic clusters as illustrated in Scheme 2. Such clusters can accommodate higher contents of water and thereby favorably enhance the conductivity. But the conductivity measurements of SPI_DSX100 membranes with very large ionic clusters could not be performed as they swell in water and loose their mechanical integrity. Similarly, PI_DSX50 membranes containing isolated water clusters [Fig. 4-1(g)] show significantly low conductivities. The above results show that the careful blending of polymer segments can significantly change the size and dispersion of ionic domains in the membranes and influence the proton conductivity.

An understanding of the proton conductivity mechanism can be obtained by examining the activation energy ($E_a$). The com-

**Table 2**
Methanol transport properties of composite membranes and Nafion117.

| Polymer code | Methanol permeability ($\times 10^{-7}$ cm$^2$ s$^{-1}$) | Methanol volume fraction, $\phi_M$ | Methanol self-diffusion coefficient, $D_M$ ($\times 10^{-7}$ cm$^2$ s$^{-1}$) | ***d***-Spacing (nm) |
|---|---|---|---|---|
| SPI | 2.18 | 0.31 | 7.03 | 9.99 |
| SPI_DSX10 | 3.41 | 0.39 | 8.74 | 10.62 |
| SPI_DSX20 | 3.49 | 0.41 | 8.51 | 9.61 |
| SPI_DSX30 | 4.11 | 0.51 | 8.05 | 8.68 |
| SPI_DSX40 | 4.22 | 0.49 | 8.61 | 8.99 |
| SPI_DSX50 | 4.54 | 0.53 | 8.56 | 9.15 |
| SPI_DSX75 | 8.54 | 0.88 | 9.70 | 19.23 |
| PI_DSX50 | 3.89 | 0.25 | 15.56 | NM |
| Nafion117 | 17.68 | 0.33 | 53.57 | NM |

"NM" not measured.

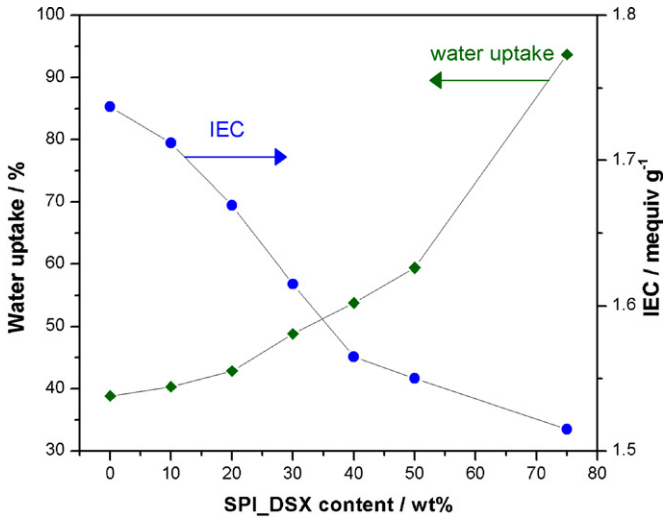


**Fig. 5.** The water uptake, IEC of composite membranes as a function of SPI_DSX amount.

posite membranes show more activation energy in composite membranes than Nafion117, indicating that the increase in conductivity with temperature is more rapid for composite membranes than for Nafion117. This result may be related to the progressive shift to vehicle-type proton conductivity from Grotthus-type under hydrated conditions [37,38]. In this regard, SPI_DSX75 (lowest IEC has highest water uptake for SPI_DSX% series, Table 1) and Nafion117 have similar proton conductivities at 90 °C, indicating at high temperature the vehicle mechanism dominates over the Grotthus mechanism [39].

### 3.6. Methanol permeability

According to the vehicle mechanism, a proton can combine with molecules such as water and methanol to form complex ions like $H_3O^+$ and $CH_3OH_2^+$. Thus, the protons can be carried together with these complex ions. Larger molecules such as methanol can permeate only through relatively broader hydrophilic channels [18]. Methanol diffusion through the polymer electrolyte membranes can be controlled by factors, such as: narrower hydrophilic channels, a lower water uptake, compact membrane structures and other operating conditions. Table 2 lists the methanol permeability

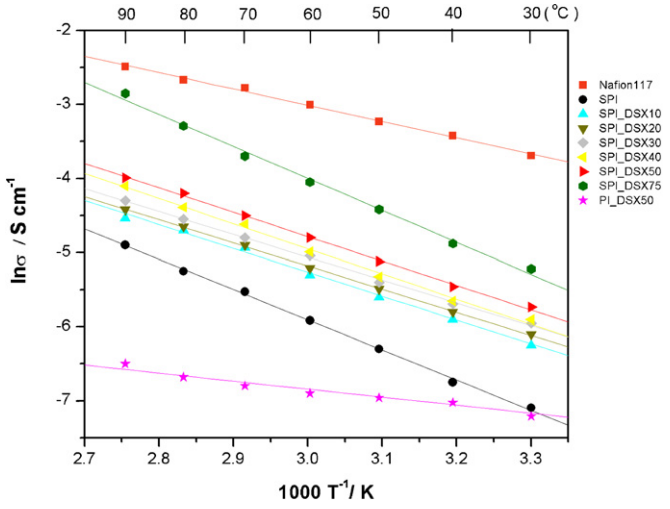


**Fig. 6.** Proton conductivity of composite membranes and Nafion117 membrane as a function of temperature, at 100% relative humidity.

of the obtained membranes at room temperature. The composite membranes showed lower values comparable to that of Nafion117 ($1.7 \times 10^{-6}$ cm$^2$ s$^{-1}$). However, these results are slightly higher than that obtained for SPI. For example, the SPI_DSX50 membrane exhibits a methanol permeability of $4.54 \times 10^{-7}$ cm$^2$ s$^{-1}$ as opposed to $2.18 \times 10^{-7}$ cm$^2$ s$^{-1}$ for SPI counterpart. For fully hydrated membranes, methanol transport across the membrane should be strongly dependent upon the water uptake because the methanol permeates through the membranes as $H_3O^+$ and $CH_3OH_2^+$. The composite membranes presented higher water uptake values and thus higher methanol permeability as compared to SPI.

In order to understand the selectivity of the prepared membranes for protons over methanol, an investigation was carried out measuring the methanol self-diffusion coefficient of the composite membranes and Nafion117. The methanol self-diffusion coefficients are shown in Table 2. According to a pulsed field gradient spin-echo $^1$H-NMR measurement, the $D_M$ for Nafion117 is reported to be $3.8–5.39 \times 10^{-6}$ cm$^2$ s$^{-1}$ [40,41], which is similar to that of our value ($5.35 \times 10^{-}$ cm$^2$ s$^{-1}$). A comparison of methanol self-diffusion coefficients reveals that SPI has the lowest diffusion coefficient. SPI_DSX75 exhibits value $9.7 \times 10^{-7}$ cm$^2$ s$^{-1}$, which is higher than SPI but lower than Nafion117. This result can be very well correlated to both the water uptake and the tortuosity of the membranes. It is well known that perfluorosulfonic polymers (here Nafion117) have a distinct separation between the hydrophilic and hydrophobic domains and therefore they form wider water-filled channels [42,43]. On the other hand, aromatic polymer electrolyte membranes containing hydrocarbon polymers have more branched channels with dead-end pockets because of the less hydrophobic nature of polymer backbone [38]. Such membrane microstructures can restrict fuel (methanol) permeation. An increase in methanol permeability and methanol diffusion coefficient in the composite membranes can be correlated to the increasing levels of water and free water in membrane. The increase in the free water content is an indication of growing hydrophilic domains and such domains allow more fuel crossover. Zou et al. also reported similar trends in membrane hydration in the siloxane incorporated sulfonated polyimide [17].

## 4. Conclusion

A series of composite membranes that consisted of sulfonated polyimide and siloxane segments were synthesized. The introduction of flexible siloxane segments improved the proton conductivity significantly. The highest proton conductivity $5.78 \times 10^{-2}$ S cm$^{-1}$ was obtained for SPI_DSX75 at 90 °C, this value is comparable to that of Nafion117 ($8.31 \times 10^{-2}$ S cm$^{-1}$). With an increase in temperature, proton conductivity increased more rapidly in composite membranes than in Nafion117. Due to the existence of bulky ionic groups and flexible siloxane segments, more water can be accommodated in the prepared membranes. The methanol transport properties of the composite membranes were investigated: methanol permeability and methanol self-diffusion coefficients ($D_M$) were found to be lower for the prepared membranes compared to Nafion. SAXS results also showed the ***d***-spacing values corresponding to narrower channels in the composite membranes. Morphology analysis revealed that the ionic clusters form well-connected hydrophilic channels which favor proton conduction. The water sorption, proton conductivity and methanol permeability were found to be governed by the size and density of the ionic clusters.

## References

[1] N. Miyake, J.S. Wainright, R.F. Savinell, J. Electrochem. Soc. 148 (2001) A898.

[2] G. Inzelt, M. Pineri, J.W. Schultze, M.A. Vorotyntsev, Electrochim. Acta 45 (2000) 2403.
[3] Y. Li, F. Wang, J. Yang, D. Liu, A. Roy, S. Case, J. Lesko, J.E. McGrath, Polymer 47 (2006) 4210.
[4] X. Zhang, S. Liu, L. Liu, J. Yin, Polymer 46 (2005) 1719.
[5] K.B. Wiles, F. Wang, J.E. McGrath, J. Polym. Sci. A: Polym. Chem. 43 (2005) 2964.
[6] D.S. Kim, H.B. Park, J.Y. Jang, Y.M. Lee, J. Polym. Sci. A: Polym. Chem. 43 (2005) 5620.
[7] P. Xing, G.P. Robertson, M.D. Guiver, S.D. Mikhailenko, S. Kaliaguine, Macromolecules 37 (2004) 7960.
[8] P. Xing, G.P. Robertson a, M.D. Guiver, S.D. Mikhailenko, K. Wang, S. Kaliaguine, J. Membr. Sci. 229 (2004) 95.
[9] Y. Okazaki, S. Nagaoka, H. Kawakami, J. Polym. Sci. B: Polym. Phys. 45 (2007) 1325.
[10] Y. Yin, O. Yamada, S. Hayashi, K. Tanaka, H. Kita, K.I. Okamoto, J. Polym. Sci. A: Polym. Chem. 44 (2006) 3751.
[11] Y. Li, R. Jin, Z. Cui, Z. Wang, W. Xing, X. Qiu, X. Ji, L. Gao, Polymer 48 (2008) 2280.
[12] W. Jang, S. Choi, S. Lee, Y. Shul, H. Han, Polym. Degrad. Stab. 92 (2007) 1289.
[13] N. Asano, M. Aoki, S. Suzuki, K. Miyatake, H. Uchida, M. Watanabe, JACS 128 (2006) 1762.
[14] J. Fang, X. Guo, S. Harada, T. Watari, K. Tanaka, H. Kita, K.I. Okamoto, Macromolecules 35 (2002) 9022.
[15] C. Lee, S. Sundar, J. Kwon, H. Han, J. Polym. Sci. A: Polym. Chem. 42 (2004) 3612.
[16] Y.A. Gallego, S.P. Nunes, A.E. Lozano, J.G. de la Campa, J. de Abajo, Macromol. Rapid Commun. 28 (2007) 616.
[17] L. Zou, S. Roddecha, M. Anthamatten, Polymer 50 (2009) 3136.
[18] C.H. Lee, H.B. Park, Y.S. Chung, Y.M. Lee, B.D. Freeman, Macromolecules 39 (2006) 755.
[19] H.J. Kim, S.Y. Cho, S.J. An, Y.C. Eun, J.Y. Kim, H.K. Yoon, H.J. Kweon, K.H. Yew, Macromol. Rapid Commun. 25 (2004) 894.
[20] H.S. Lee, A. Roy, O. Lane, J.E. McGrath, Polymer 49 (2008) 5387.
[21] P.R. Sukumar, W. Wu, D. Markova, O. Unsal, M. Klapper, K. Mullen, Macromol. Chem. Phys. 208 (2007) 2258.
[22] P.G. Romero, J.A. Asensio, S. Borros, Electrochim. Acta 50 (2005) 4715.
[23] S.K. Kim, T.H. Kim, J.W. Jung, J.C. Lee, Macromol. Mater. Eng. 293 (2008) 914.
[24] G. Gebel, Polymer 41 (2000) 5829.
[25] Y.J. Kim, W.C. Choi, S.I. Woo, W.H. Hong, J. Membr. Sci. 238 (2004) 213.
[26] V. de Zea Bermudez, L. Alcacer, J.L. Acosta, E. Morales, Solid State Ionics 116 (1999) 197.
[27] P.H. de Souza, R.F. Bianchi, K. Dahmouche, P. Judeinstein, R.M. Faria, T.J. Bonagamba, Chem. Mater. 13 (2001) 3685.
[28] Y.W. Chang, E. Wang, G. Shin, J.E. Han, P.T. Mather, Polym. Adv. Technol. 18 (2007) 535.
[29] C. Genies, R. Mercier, B. Sillion, R. Petiaud, N. Cornet, G. Gebel, M. Pineri, Polymer 42 (2001) 5097.
[30] G. Suresh, A.K. Pandey, A. Goswami, J. Membr. Sci. 295 (2007) 21.
[31] S.B. Tian, G. Xu, Polymer 36 (1995) 1555.
[32] M. Simionescu, M. Marcu, M. Cazacu, C. Racles, Eur. Polym. J. 38 (2002) 229.
[33] T.C. Chang, K.H. Wu, Polym. Degrad. Stab. 60 (1998) 161.
[34] G. Gebel, Macromolecules 33 (2000) 4850.
[35] A. Higuchi, T. Lijima, Polymer 26 (1985) 1207.
[36] D.S. Kim, H.B. Park, J.W. Rhim, Y.M. Lee, J. Membr. Sci. 240 (2004) 37.
[37] T.A. Zawodzinski Jr., M. Neeman, L.O. Sillerud, S. Cottesfeld, J. Phys. Chem. 95 (1991) 6040.
[38] K.D. Kreuer, J. Membr. Sci. 185 (2001) 29.
[39] X. Ren, S. Gottesfeld, J. Electrochem. Soc. 148 (2001) A87.
[40] X. Ren, T.E. Springer, T.A. Zawodzinski, S. Gottesfeld, J. Electrochem. Soc. 147 (2000) 466.
[41] H.A. Everya, M.A. Hickner, J.E. McGrath, T.A. Zawodzinski Jr., J. Membr. Sci. 250 (2005) 183.
[42] M. Fujimura, T. Hashimoto, H. Kawai, Macromolecules 14 (1981) 1309.
[43] M. Fujimura, T. Hashimoto, H. Kawai, Macromolecules 15 (1982) 136.